RSC Advances

PAPER

View Article Online
View Journal | View Issue

Cite this: *RSC Adv.*, 2021, **11**, 1461

Targeting self-assembled F127-peptide polymer with pH sensitivity for release of anticancer drugs†

Wenzhao Han, Fanwei Meng, Hao Gan, Feng Guo, Junfeng Ke and Liping Wang *

Received 22nd November 2020
Accepted 19th December 2020

DOI: 10.1039/d0ra09898a

rsc.li/rsc-advances

The treatment of breast cancer mainly relies on chemotherapy drugs, which present significant side effects. The most typical example is the cardiotoxicity and bone marrow suppression associated with doxorubicin (DOX). Therefore, this drug is not the first choice in clinical treatment. We designed ATN-FFPFF-ATN, a new targeted antitumor drug carrier, polymerized from phenylalanine dipeptide (FF), ATN-161 peptide, and Pluronic® F-127. The peptide and Pluronic® F-127 are linked with acetal and are, therefore, acid-sensitive. As cancer can reduce pH through complex mechanisms and subsequently maintain acid ambience, our vehicle can smartly unravel at a peculiar position, through which the drug can specifically accumulate inside the tumor. ATN-161 is a protein ligand of integrin $\alpha_5\beta_1$, which is highly expressed on the surface of some breast cancer cells. This targeting peptide sequence can play a role in the selective delivery of DOX to tumor cells. The DOX-carrying vector was able to significantly inhibit cell proliferation and promote cell apoptosis in MDA-MB-231 cells. Based on these results, ATN-FFPFF-ATN with pH response is a promising vehicle for DOX delivery.

1. Introduction

In recent years, due to an increase in obesity rate and a decrease in fertility rate, breast cancer has become one of the most common cancers among women. Breast cancer currently accounts for 30% of female cancers. The American Cancer Society (ACS) expects a further 48 530 cases of breast cancer *in situ* in 2020.[1] The main clinical treatment strategy for breast cancer is chemotherapy.[2] However, the side effects of chemotherapy drugs have a great impact on patients' lives. The most typical example is doxorubicin (DOX). As a kind of broad-spectrum antitumor drug, DOX inhibits the synthesis of DNA and RNA in tumor cells and is commonly used in the treatment of malignant tumors, such as acute leukemia, breast cancer, liver cancer, lung cancer, pancreatic cancer, and lymphoma.[3] However, it can cause severe cardiotoxicity and bone marrow suppression.[4–6]

Several studies have focused on avoiding damage to normal cells during chemotherapy treatment and the systemic toxicity caused by chemotherapy drugs.[7–9] Numerous studies show that the tumor tissue environment differs from the normal environment.[10] Specifically, the internal pressure is higher[11–13] and the pH is lower than that of normal tissues. The pH of normal tissue is 7.4, between tumor cells is 6.8, and within tumor cells is 4.5–6.5.[14] Based on this unique characteristic, antitumor drugs can be more precisely targeted to tumor tissues. This observation provides new design ideas for nano drug-loading systems.[15–17] Deng *et al.* studied pH-sensitive frizzled peptides. Peptides form opening and closing structures, similar to a zipper, which are sensitive to environmental pH by virtue of hydrophilic and hydrophobic interactions.[18] Fu *et al.* designed a pH-responsive peptide gel with a β-sheet structure. The structure of the peptide gel changed under pH 5.[19] In addition to this method, it is possible to polymerize materials together through pH-sensitive chemical bonds, including phenylimine,[20] acetal or ketal,[21] and acylhydrazone bonds.[22] Injectable shell-crosslinked F127 hydrogel composites were designed by Liu's group using tacetal polymerization of chitosan and F127, which showed a pH-dependent effect. The delivery of curcumin and 5-fluorouracil showed good antitumor effects.[23] The polymer carrier of soluble starch (St) and deoxycholic acid (DCA) designed by Yang showed efficacy in delivering DOX. The ester bond in St-DCA is acid sensitive and the drug release increased significantly at pH 5.5.[24–27] These materials are relatively stable in normal tissue environments, whereas they swell and disintegrate in acidic environments.[28] Therefore, these carriers can selectively deliver drugs and reduce damage to non-targeted tissues.

Phenylalanine dipeptide (FF) was discovered while studying Alzheimer's β-amyloid protein. Meital *et al.* found that FF is closely related to the self-assembly of β-amyloid protein.[29] Later, Li *et al.* discovered that nanospheres assembled by FF can carry oligonucleotides into cells.[30] Inspired by this, in our previous study, we observed that the survivin-siRNA carried by FF is effective in inhibiting tumor cells and promoting tumor

Key Laboratory for Molecular Enzymology and Engineering, Ministry of Education, School of Life Sciences, Engineering Laboratory for AIDS Vaccine, Jilin Universtiy, Changchun 130012, P. R. China. E-mail: wanglp@jlu.edu.cn; Tel: +86-431-8515-5348

† Electronic supplementary information (ESI) available. See DOI: 10.1039/d0ra09898a

apoptosis. Moreover, we found that FF has low cytotoxicity and high transfection efficiency.[31,32] In this study, we aimed to test if this carrier is selective for tumors. For this purpose, we designed FFPFF, which linked Pluronic® F-127 and the FF sequence through Schiff bond aggregation. Under acidic conditions, the Schiff bond was broken to make the carrier structure capable of drug dispersal, thereby enabling the release of the contained drug. To increase delivery selectivity to breast cancer cells, we improved the carrier. We linked the ATN-161 peptides to the C-terminus of the FF sequence to target the α1β5 integrin receptor on the surface of breast cancer cells and named the structure ATN-FFPFF-ATN. Furthermore, we inserted two alanines between the FF and ATN-161 sequences to avoid steric hindrance between the two sequences. At least 24 integrins have been discovered, including 18α subunits and 8β subunits. Among them, integrins $\alpha_v\beta_3$, $\alpha_v\beta_5$, and $\alpha_5\beta_1$ play a role in regulating tumor cell growth, metastasis, and angiogenesis. Integrin $\alpha_5\beta_1$ is highly expressed on the surface of many tumor cells. Therefore, integrin peptide ligands appear promising in drug delivery. ANT-161, an integrin protein receptor, can specifically recognize integrin $\alpha_5\beta_1$.[33] In a study by Dai, ATN-161 was attached to a liposome carrier to deliver DOX to HUVEC (human umbilical vein endothelial cells) and MDA-MB-231 (breast cancer cells). This study showed that this targeted delivery improves the transfection efficiency of cells and can reduce the drug dosage.[34] Zhang *et al.* reported that the functionalized ATN-161 peptide polymer effectively delivers DOX during the treatment of melanoma. The study found that ATN-161 peptide played a significant targeting role in both *in vivo* and *in vitro* experiments.[35]

Herein, we loaded FFPFF and ATN-FFPFF-ATN with DOX. After the polymer self-assembles, it can form a shell composed of hydrophilic groups and a core composed of hydrophobic groups. DOX was entrapped in the hydrophobic core during hydrophobic self-assembly. Then we tested whether the drug-loading carrier was able to inhibit proliferation and promote apoptosis in MDA-MB-231 cells.

2. Experimental

2.1 Materials

Fmoc-Phe-OH, Fmoc-Pro-OH, Fmoc-His(Trt)-OH, Fmoc-Cys(Trt)-OH, Fmoc-Asn(Trt)-OH, Fmoc-Lys(Boc)-OH, Fmoc-Ala-OH, Rink amide-AM resin, 1-hydroxybenzotriazole, benzotriazole-1-yl-oxytripyrrolidinophosphonium hexafluorophosphate, and N-methylmorpholine were obtained from GL Biochem (Shanghai, China). Dimethylformamide, methanol, dichloromethane, and *n*-hexane were obtained from Beijing Chemical Factory (Beijing, China). Pluronic® F-127 and DMSO were obtained from Sigma-Aldrich (St. Louis, MO, USA). Dess–Martin periodinane was provided by Aladdin (Shanghai, China). DMEM medium was purchased from Thermo Fisher Scientific (Shanghai, China). Fetal bovine serum was purchased from Kang Yuan Biology (Tianjin, China). Trypsin and Hoechst 33258 nuclear dye were obtained from Solarbio (Beijing, China). Thiazolyl blue tetrazolium bromide (MTT) was purchased from Genview (Beijing, China). WST-1 kit and Lysotraker Green procured from Beyotime (Shanghai, China). Annexin V-FITC/PI apoptosis detection kit was purchased from BestBio (Shanghai, China).

2.2 Synthesis, purification, and characterization of the polymers

The hydroxyl end of Pluronic® F-127 (F127) was oxidized to the aldehyde group using Dess–Martin reagent.[23] First, 5.16 g of F127 was stirred and completely dissolved in 410 mL of dichloromethane. Thereafter, 0.5 g of Dess–Martin reagent was added and stirred in water at 40 °C for 24 h. The product was separated out using *n*-hexane and then dialyzed and lyophilized. It was stored at −20 °C until further use. The degree of oxidation of F127 was calculated using ^{1}H-NMR.

FF (Ac-Phe-Phe-NH_2), ATN-AAFF (Ac-Pro-His-Ser-Cys-Asn-Lys-Ala-Ala-Phe-Phe-NH_2), and ATN-161 (Ac-Pro-His-Ser-Cys-Asn-Lys-NH_2) were synthesized using solid-phase peptide synthesis with standard Fmoc strategy on Rink Resin. The crude peptides were identified using liquid chromatography (LCMS, SHIMADZU, Kyoto, Japan). Coupling of amino acids was carried out using dichloromethane (DMF) by loading amino acids one by one from the C-terminus to the N-terminus. The peptide sequences and F127-CHO (molar ratio 5 : 1)[36] at pH 4.5 and 25 °C were stirred in ethanol for 24 h using a magnetic stirrer to form Schiff bond, using molecular sieve and magnesium sulfate to absorb water and promote the reaction. Dialysis was performed at 25 °C for 24 h to remove unloaded peptide. Ethanol was removed using rotary evaporation, and the product was freeze-dried. The polymers were identified using ^{1}H-NMR (BRUKER, AVANCEIII500) and a Fourier transform infrared (FTIR) (Vertex 80v, Bruker, Billerica, MA, USA).

The polymer was dissolved to yield the desired concentration and sonicated for 30 min to complete the self-assembly. The morphology of self-assembly was observed using scanning electron microscopy (SEM) (S-4800, Hitachi, Tokyo, Japan) and transmission electron microscopy (TEM) (JEM-2200FS, JEOL Ltd, Tokyo, Japan). A dynamic light scattering instrument (NANO ZS90, Malvern Panalytical, Malvern, UK) was used to detect the particle size and zeta potential of self-assembled polymers.

2.3 Preparation of DOX-loaded the polymers

DOX liquor was prepared by dissolving 10 mg DOX·Cl in 2 mL DMSO, followed by the addition of 25 μL of triethylamine for desalting; the mixture was stirred for 2 h in the dark. DOX solution was slowly dropped into the polymer carrier solution while being stirred magnetically for 2 h at 25 °C. Drug-loaded polymers were prepared with a theoretical drug loading of 5, 10, and 20%. Ultrasound was performed for 30 min to complete the self-assembly behavior of the carrier. Dialysis was performed at 25 °C for 24 h to remove unloaded DOX, triethylamine hydrochloride, and DMSO. The freeze-dried product was sealed and stored at −20 °C. The calculation formula of load capacity (DLC) and load efficiency (DLE) is as follows:

$$\text{Load capacity (\%)} = \frac{\text{DOX in the polymer (mg)}}{\text{Drug loaded polymer (mg)}} \times 100$$

$$\text{Load efficiency (\%)} = \frac{\text{DOX in the polymer (mg)}}{\text{Total DOX in formulation (mg)}} \times 100$$

2.4 *In vitro* drug release

PBS buffers with pH of 7.4 and 5.5 were used to configure two polymer-carriers each with a concentration of 1 mg mL^{-1}. Each solution (5 mL) was taken in a pretreated dialysis bag (MW 1 kDa), suspended in a centrifuge bucket containing 50 mL of the corresponding pH PBS buffer, and magnetically stirred at a constant temperature of 37 °C. At the set time, 1 mL of dialysate was taken and 1 mL of fresh PBS at the corresponding pH was added to the dialysate. The absorbance of DOX was determined at each time point in each group at 480 nm using a UV spectrophotometer (UV2501, SHIMADZU). DOX cumulative release formula can be represented as follows:

$$\text{Cumulative release of DOX} = \frac{50 \times C_n + 1 \times \Sigma C_{n-1}}{\text{DOX in the polymer}} \times 100\%$$

C_n and C_{n-1} represent the concentration of DOX (mg mL^{-1}) in the dialysate taken n and $n-1$ times, respectively.

2.5 Cell culture and *in vitro* cytotoxicity of the polymers

The breast cancer cell line, MDA-MB-231, with high expression of integrin $\alpha_5\beta_1$ protein receptor, was cultured in DMEM supplemented with 10% fetal bovine serum, 100 U mL^{-1} penicillin, and 100 μg mL^{-1} streptomycin in an incubator at 37 °C in a 5% CO_2 environment.

A 96-well plate was plated one day before the experiment and cells were seeded at a density was 5×10^3 cells per well. The experimental concentration of the polymer carrier to be tested was added on the day of the experiment. Four parallel wells were set for each experimental concentration. After 24 or 48 h of incubation, 10 μL of MTT solution (5 mg mL^{-1}) was added to each well. After incubating for 4 h, the liquid was slowly aspirated from each well and 150 μL of DMSO was added to each well. The plate was placed at a constant temperature shaker at 37 °C for 10 min. The absorbance at 490 nm was detected using a microplate reader (Bio-Rad Laboratories, Hercules, CA, USA).

2.6 Cellular uptake of the polymers

Cell transfection was detected using flow cytometry. MDA-MB-231 cells were seeded in a 6-well plate at a density of 5×10^6 cells per well and cultured for 24 h. The competitive inhibition group was incubated with ATN-161 peptide (1 mg mL^{-1}) for 4 h and then washed with PBS. Next, experimental peptides were added to the corresponding wells at a final DOX concentration of 20 μg mL^{-1}. After culturing for 4 h, the medium in each well was removed and the wells were washed with PBS. Cells in each well were digested, centrifuged (600 rpm, 5 min), and resuspended in 500 μL PBS. Flow cytometry (Accuri C6, BD Biosciences, San Jose, CA, USA) and confocal microscopy were used to determine cell transfection. MDA-MB-231 cells with a density of 2×10^4 cells per dish were poured in a dedicated culture dish and cultured for 24 h. The cell dosing protocol was similar to that previously described in this section. After the cells were transfected for 4 h, the medium in each well was removed and washed with PBS. The cells were fixed using 4% paraformaldehyde and then stored overnight at 4 °C. Next, the cells were washed with PBS five times and Hoechst 33258 was added to stain the cell nuclei for 15 min. The cells were washed five times with PBS after the dye was removed. Laser scanning

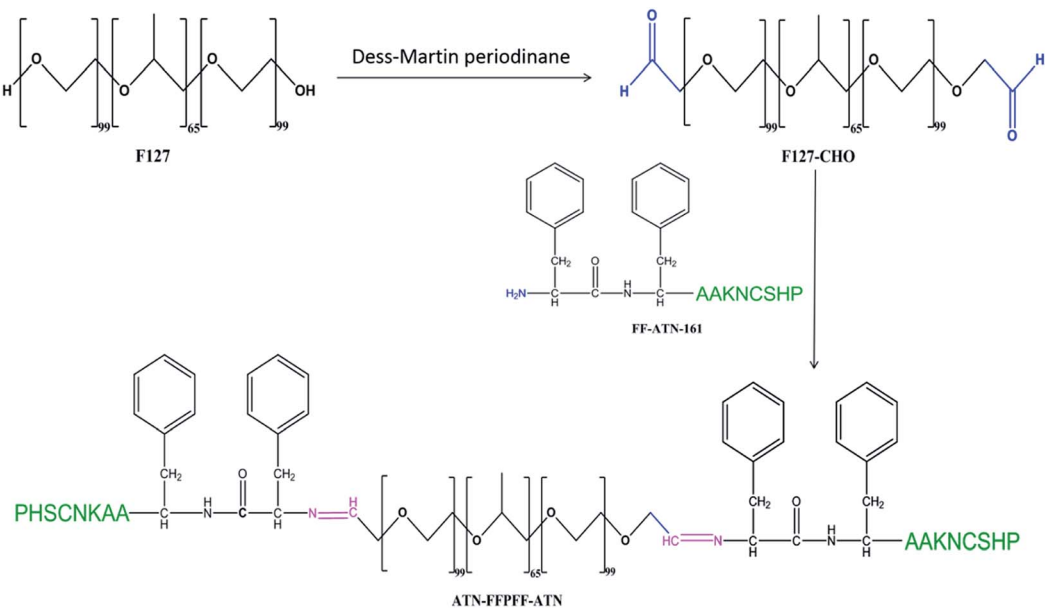

Scheme 1 The synthesis scheme of ATN-FFPFF-ATN.

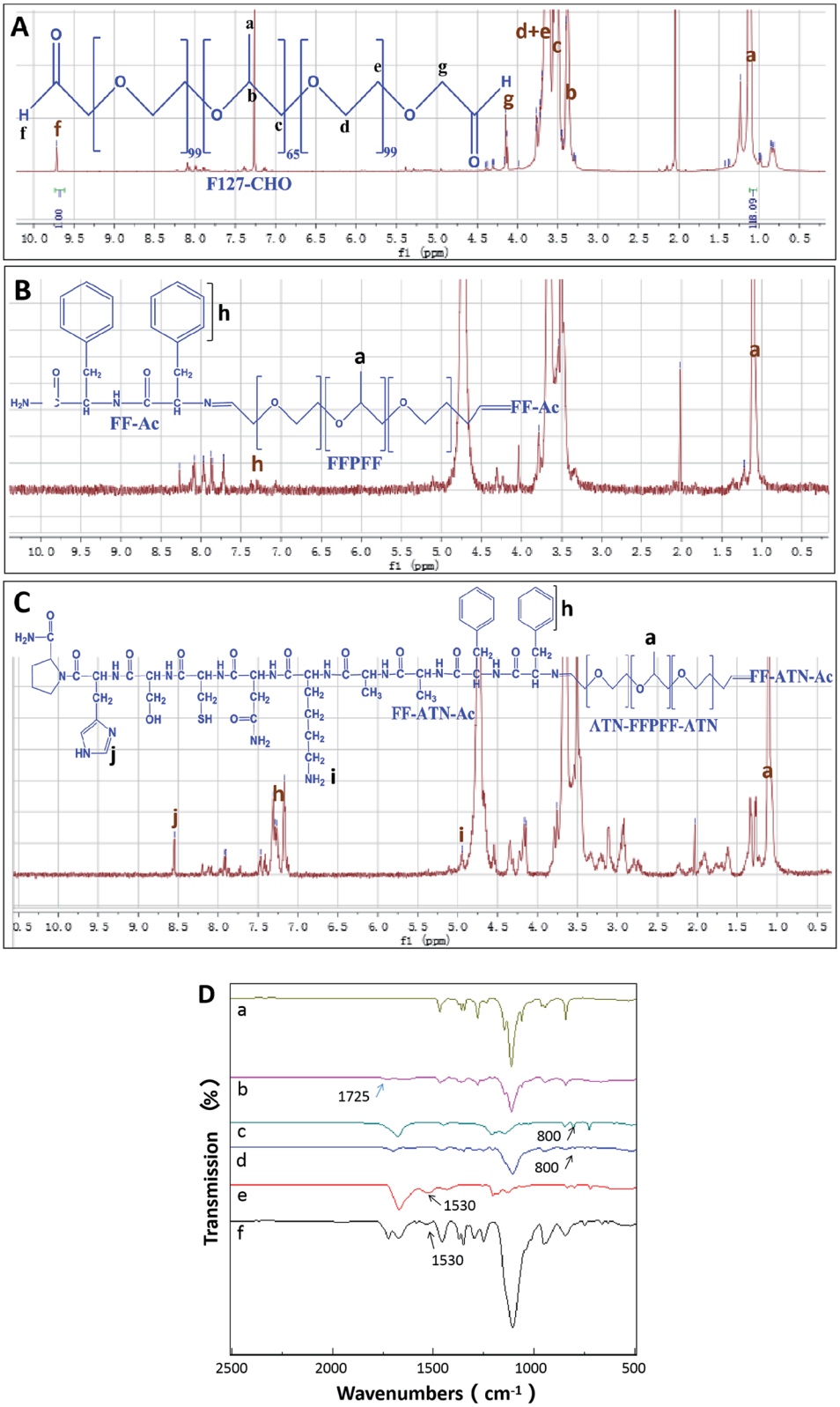

Fig. 1 ^{1}H NMR spectrum of F127-CHO spectrum (A), FFPFF spectrum (B), ATN-FFPFF-ATN spectrum (C); (D) FTIR spectra of F127 (a), F127-CHO (b), FF (c), FFPFF (d), ATN-161 (e), and ATN-FFPFF-ATN (f).

confocal microscope (LSM710, Zeiss, Oberkochen, Germany) was used to observe and capture images. Lysotracker staining is to incubate the cells with a final concentration of 200 nM dye at 37 °C for 10 min before the cells are fixed.

2.7 *In vitro* antitumor activity assay

The inhibitory effect on tumor cells was assessed using a WST-1 kit. A 96-cell well plate was prepared the day before the experiment and seeded with MDA-MB-231 at a density of was 5×10^3 cells per well. On the day of the experiment, a DOX-loaded carrier or free-DOX was added and four parallel wells were set in each group. The inhibition experiment was carried out by using free ATN-161 to pretreated cells for 4 h before adding ATN-FFPFF-ATN-DOX. MDA-MB-231 cells incubation with formulations (DOX 20 μg mL^{-1}) in 4 h, and then replace the drug-free medium and continue culturing for 20 hours. Then, 10 μL of WST-1 working solution was added, and after 1 h of incubation, the absorbance at 690 nm was measured using a microplate reader. An Annexin V-FITC cell apoptosis kit was used to determine apoptosis. Cell culture and drug-delivery methods were similar to that described under flow cytometry. To suspend the cells, 400 μL of 1× Annexin V binding solution was added, and 5 μL of Annexin V-FITC staining solution was then added, mixed well, and incubated on ice for 15 min in the dark. Lastly, 5 μL of PI staining solution was added, mixed well, and incubated in the dark for 5 min. Flow cytometry was carried out within an hour of incubation.

2.8 Statistical analysis

Data were analyzed using GraphPad Prism8 software (GraphPad Software, San Diego, CA, USA). Differences between two groups were compared using Student's *t*-test. P values <0.05 were considered statistically significant.

3. Results and discussion

3.1 Synthesis and characterization of the polymers

The peptides synthesized using solid-phase peptide synthesis were verified using LCMS, as shown in Fig. S1.† The purity and molecular weights were consistent with the calculated and expected values. The synthesis process of ATN-FFPFF-ATN is shown in Scheme 1. The structure of FFPFF and ATN-FFPFF-ATN were confirmed using ^{1}H-NMR and FTIR. As shown in Fig. 1A, the proton peak on the aldehyde group appeared at 9.71 ppm. The areas of the two proton peaks at 9.71 ppm (–CHO) and 1.11 ppm ($OCH_2OH(CH_3)O$) were calculated using integration[19] and the degree of oxidation of PF-127-CHO was about 83%. FFPFF showed the peaks of FF at 7.21–7.33 ppm ($–CHCH_2C_6H_5$) and the peak at 9.71 ppm disappeared, confirming that the F127-CHO was successfully crosslinked by FF (Fig. 1B). ATN-FFPFF-ATN showed the characteristic peak of imidazolyl at 8.62 ppm (NHCHNCH–) and the peak of amino on Lysine at 5.02 ppm ($–NH_2$), similarly the peak at 9.71 ppm disappeared. This proved that both sides of F127-CHO are confirmed to be conjugated by ATN-161-AA-FF (Fig. 1C). As shown in Fig. 1D, the spectrum of F127-CHO shows a new peak

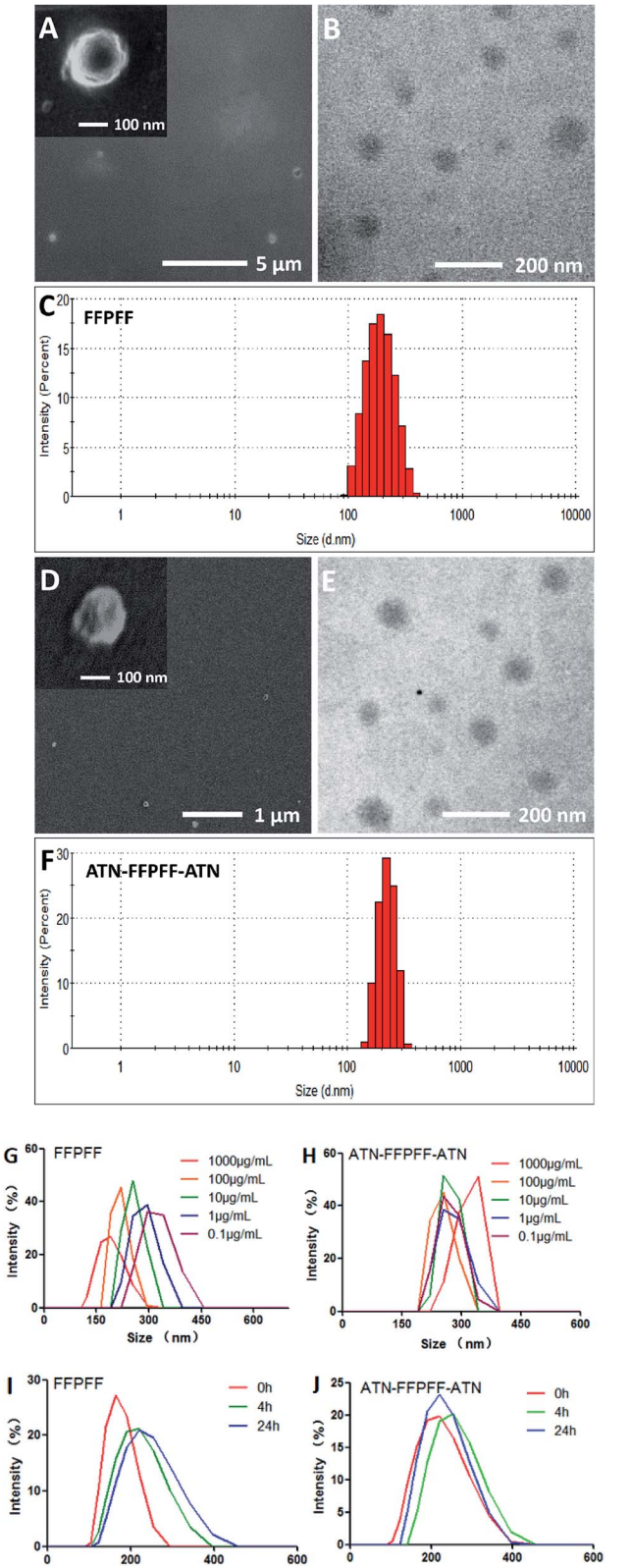

Fig. 2 (A and B) SEM and TEM images of FFPFF at a concentration of 100 μg mL^{-1} (D and E) SEM and TEM images of ATN-FFPFF-ATN at a concentration of 100 μg mL^{-1} (C and F) Particle size of FFPFF and ATN-FFPFF-ATN (100 μg mL^{-1}). Dilution stability of FFPFF (G) and ATN-FFPFF-ATN (H). Time stability of FFPFF (I) and ATN-FFPFF-ATN (J).

Table 1 The particle size and zeta at pH 5.5 and 7.4

	pH	Size (nm)	Zeta (mV)
FFPFF 100 μg mL^{-1}	7.4	195.7	−18.1
	5.5	490.4	0.199
ATN-FFPFF-ATN 100 μg mL^{-1}	7.4	255.3	−19
	5.5	896.6	0.182

at 1725 cm^{-1} (C═O stretching of the aldehydes), which indicated that some of the primary alcohols had been successfully oxidized to aldehydes. However, the peak at 1725 cm^{-1} disappeared in the FTIR spectra of FFPFF and ATN-FFPFF-ATN. FFPFF showed a new peak at 800 cm^{-1} which was attributed to a benzene ring, and ATN-FFPFF-ATN showed a new peak at 1530 cm^{-1} which was attributed to imidazolyl, suggesting the aldehydes groups in the F127-CHO reacted with the amino groups in the peptides.

The scanning electron microscopy (SEM) and the transmission electron microscopy (TEM) revealed FFPFF (100 μg mL^{-1}) nanospheres with uneven surface structures, as seen in Fig. 2A and B. The dynamic light scattering (DLS) revealed the particle size to be 195.7 nm (PDI = 0.389) (Fig. 2C), and the zeta potential was determined to be −18.1 mV. ATN-FFPFF-ATN was observed and it also exhibited a nanosphere structure, although the surface protrusions were more obvious, which may be attributed to the conformation of the targeting peptide as shown in Fig. 2D and E. The particle size of ATN-FFPFF-ATN was 255.3 nm (PDI = 0.522) as seen in Fig. 2F. The peptides of ATN-161 were mainly hydrophilic amino acids, which might have opposed the internal hydrophobic forces of the nanospheres and caused an increase in the diameter. The zeta potential of ATN-FFPFF-ATN was −19 mV. The dilution stability of the two polymer carriers is shown in Fig. 2G and H. The average particle size of FFPFF gradually increased with dilution; it increased to 294.3 nm in 0.1 μg mL^{-1}. In contrast, the particle size of ATN-FFPFF-ATN did not change significantly during the dilution process. In time stability, ATN-FFPFF-ATN also performed better. As shown in Fig. 2I and J, within 24 h, the average particle size of ATN-FFPFF-ATN did not change significantly. In general, the particle size of the carrier does not change significantly, which may be ascribed to PEG in F127.[37]

3.2 pH responsiveness of the polymers

During the design of the carrier material, the peptide and F127 were linked by a Schiff bond, which is stable under neutral and alkaline conditions and can be broken under acidic conditions.[38] Therefore, the carrier material of the matrix can stably contain the internal drug in normal tissue and blood (pH 7.4), while the drug-containing carrier will collapse in the tumor cell (pH 4.5–6.5). This allows the targeting of the drug to tumor cells while reducing their effects on normal tissues. In our study, PBS with pH 7.4 and 5.5 was used to configure two polymer self-assemblies with a concentration of 100 μg mL^{-1} and the particle size and surface potential of each experimental group were measured. Table 1 shows that the particles of the two polymers increased significantly in pH 5.5. These findings indicated that in an acidic environment, the rupture of the Schiff bond reduced the stability of the self-assembled structure and resulted in structural expansion. In addition, the surface potential also changed significantly, which indicated that the stability of the colloidal dispersion decreased.

In addition, the two carriers treated with pH 5.5 were observed using TEM and the results are shown in Fig. 3A and B. Under acidic conditions, both carriers showed structural disintegration, an obvious increase in particle size.

3.3 Drug loading of the polymers and *in vitro* drug release

DOX is a hydrophobic drug that can be incorporated into the carrier core during the self-loading process.[39] We calculated

Table 2 Characteristics of FFPFF-DOX and ATN-FFPFF-ATN-DOX at 20 wt% theoretical DOX loading content

	Theoretical DLC (wt%)	DLC (wt%)	DLE (wt%)
FFPFF-DOX	20	18.33	91.64
ATN-FFPFF-ATN-DOX	20	19.53	97.65

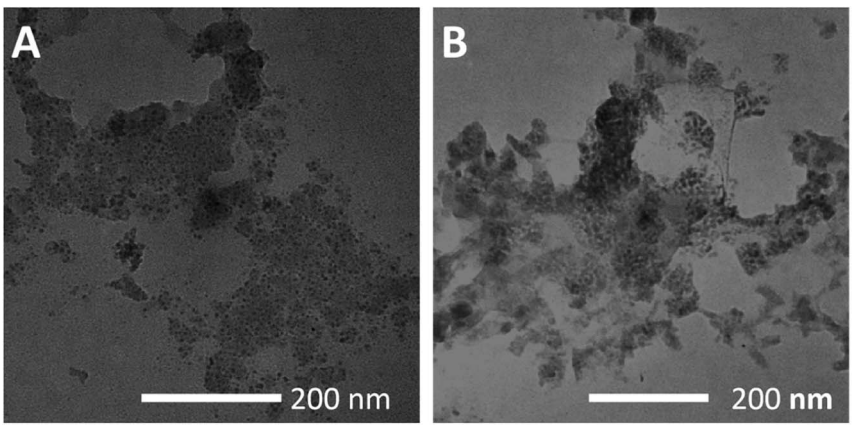

Fig. 3 TEM images of FFPFF (100 μg mL^{-1}) (A) and ATN-FFPFF-ATN (100 μg mL^{-1}) (B) at pH 5.5.

DLC and DLE for theoretical drug loading of 5, 10, and 20%. The comprehensive comparison revealed that drug loading and the rate of drug loading were optimum at the theoretical drug loading of 20%. Therefore, for subsequent experiments, the theoretical drug loading of 20% was chosen. The drug loading and drug-loading rates for the two carriers are shown in Table 2.

The results of *in vitro* release of DOX are presented in Fig. 4, which shows that the drug release of the two carriers at pH 5.5 increased significantly. The FFPFF and ATN-FFPFF-ATN drug-loaded drug release reached 41.53 and 44.87%, at 3 h, respectively. At the same time, 12.07 of FFPFF and 7.17% of ATN-FFPFF-ATN were released, at pH 7.4. At 24 h, the FFPFF drug release rate at pH 5.5 was 66.60%, ATN-FFPFF-ATN was 59.09%. FFPFF drug-release rate at pH 7.4 was 39.21%, while that of ATN-FFPFF-ATN was 31.51%. There were significant differences in the cumulative release rate between the two polymer-carriers at pH 7.4 and 5.5. From the above data analysis, it can be inferred that the carrier was beneficial to the release of the drug in an acidic environment.

3.4 *In vitro* cytotoxicity of the polymers

We chose MDA-MB-231 cell line with high expression of the integrin $\alpha_5\beta_1$ protein as the targeting cell model, MCF-7 cell line as the non-targeted model. We performed an *in vitro* cytotoxicity test on the empty vector. The results are shown in Fig. 5. The survival rates of FFPFF and ATN-FFPFF-ATN cells at the maximum concentration after 24 h were 90.72 and 91.93%, respectively, in MDA-MB-231 cells. Further analysis found that the two vectors had no significant difference in cell-survival rate in MDA-MB-231 cells, which proved that the targeting peptide sequence would not cause additional inhibition of cell proliferation. This is consistent with the conclusion reported in the literature that ATN-161 has no antitumor effect *in vitro*.[34] Similar results were seen in MCF-7 cells, in which the survival rates of FFPFF and ATN-FFPFF-ATN cells at 100 μg mL^{-1} concentration after 24 h were 88.79% and 87.40%, respectively. It is also very important to evaluate the toxicity of carrier materials in the blood circulation process.[40] In HUVEC cells, the survival rates of FFPFF and ATN-FFPFF-ATN at 100 μg mL^{-1} were 91.18% and 91.10%. Therefore, it can be speculated that the carrier will be biocompatible to vascular endothelial cells in the blood circulation.

3.5 Cellular uptake of the polymers

In this part of the experiment, the effectiveness of internalization and targeting was assessed with MDA-MB-231 cells. It can be seen in the laser scanning confocal microscope (CLSM) image (Fig. 6A) that DOX emitted red fluorescence, while the nucleus was blue. The cells in the control group did not emit red fluorescence, while the other four groups showed red fluorescence with different brightness intensities. It can be deduced from Fig. 6A that DOX was able to enter the cells after a 4 h incubation period. When comparing FFPFF-DOX and ATN-FFPFF-ATN-DOX, it could be seen that the red fluorescence intensity of the targeted group was greater than that of the non-targeted group. This showed that the ATN-161 targeting peptide

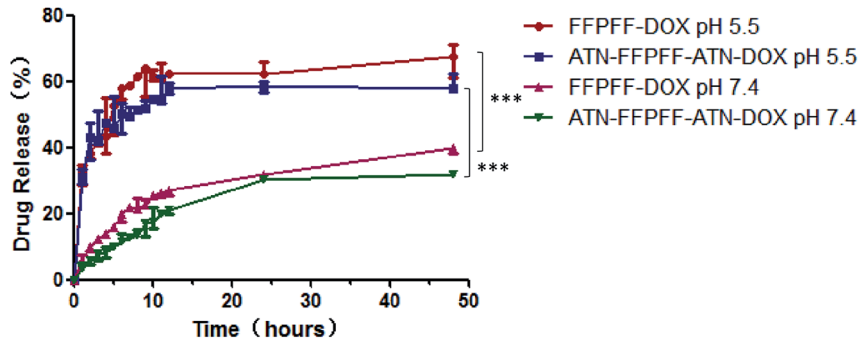

Fig. 4 Release profile of DOX at pH 7.4 and pH 5.5. *p < 0.05, **p < 0.01, ***p < 0.001.

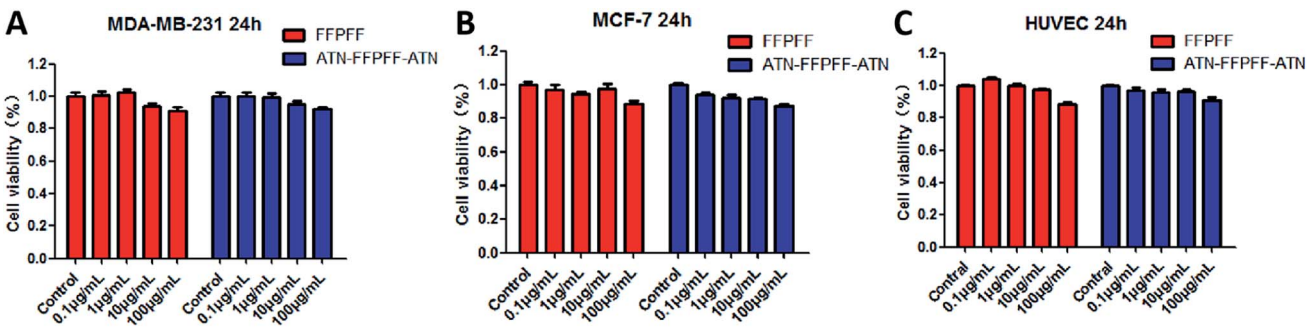

Fig. 5 Cell viability of MDA-MB-231 (A) MCF-7 (B) HUVEC (C) cells was determined with different concentrations of FFPFF and ATN-FFPFF-ATN for 24 h.

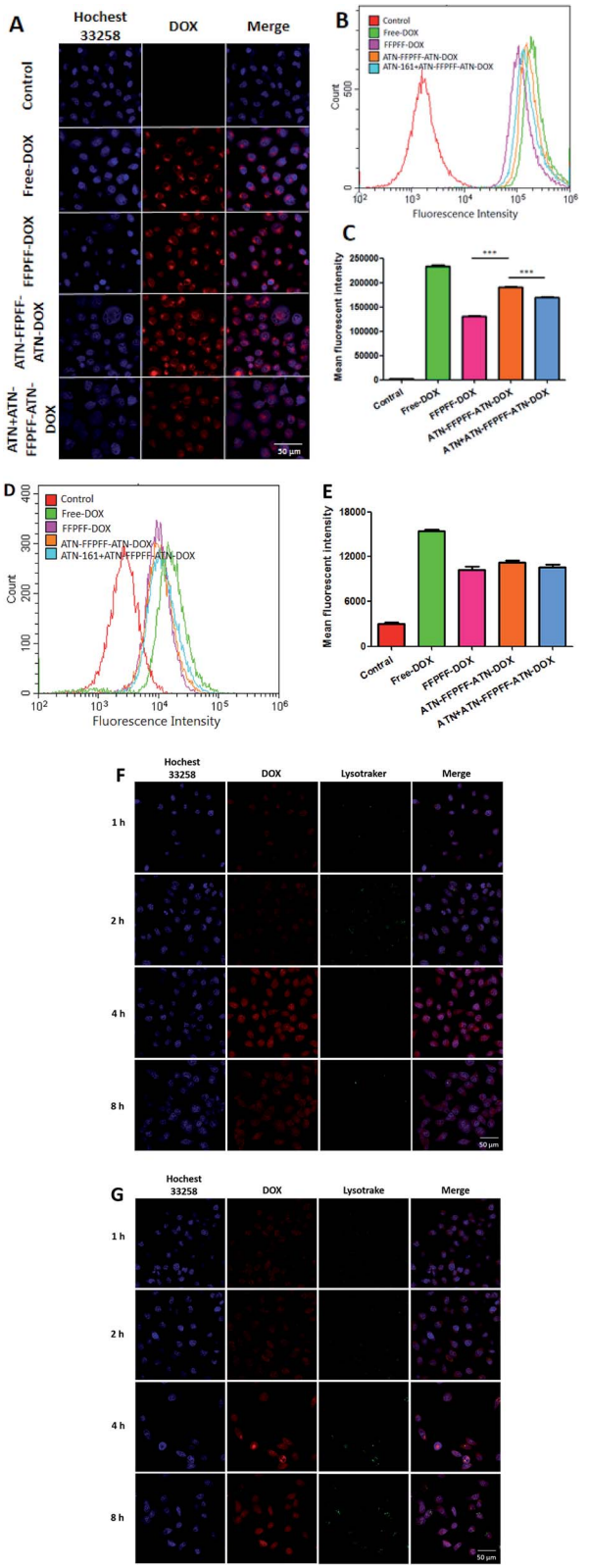

Fig. 6 (A) Confocal microscopy images of MDA-MB-231 cells after incubation for 4 h (magnification: 400×). The inhibition experiment was carried out by using free ATN-161 to pretreat cells for 4 h before adding ATN-FFPFF-ATN-DOX. (B) Flow cytometric analysis of MDA-MB-231 cells for 4 h incubation. (C) The mean fluorescence intensities of B. (D) Flow cytometric analysis of MCF-7 cells for 4 h incubation. (E) The mean fluorescence intensities of D. The co-localization capabilities of the nucleus, DOX and lysosome in MDA-MB-231 cells delivered by FFPFF-DOX (F) and ATN-FFPFF-ATN-DOX (G) for different time. *$p < 0.05$, **$p < 0.01$, ***$p < 0.001$.

played a role in the process of cell transfection. In addition, in order to further verify the effect of the targeting peptide, we set up a targeted competition inhibition group. The cells were incubated with the ATN-161 peptide first, so that the integrin $\alpha_5\beta_1$ protein on the MDA-MB-231 cells was bound to the ATN-161 peptide. Results revealed that the red fluorescence of the targeted competitive inhibition group was significantly weaker than that of the ATN-FFPFF-ATN group. This proved that the ATN-161 peptide had a specific targeting effect on the integrin $\alpha_5\beta_1$ protein.

We performed a quantitative analysis using flow cytometry and the results are seen in Fig. 6B. The free-DOX group had the strongest fluorescence intensity, which might have occurred due to the small size of the free DOX molecules, which were able to enter cells through passive diffusion. This method was faster than endocytosis; therefore, the amount of DOX was highest. In addition, when the other three groups were compared, it could be seen that the fluorescence intensity of the ATN-FFPFF-ATN targeting group was greater; our findings were similar to those from CLSM, indicating that the targeting sequence could play a targeting role and promote cell transfection. We did the same experiment in nonselective cells (MCF-7), and the results are demonstrated in Fig. 6D. There was no significant difference between FFPFF ATN-FFPFF-ATN and ATN + ATN-FFPFF-ATN in MCF-7 cells. This means that in non-targeted cells, there is no interaction between the targeting peptide sequence and the receptor on the cell membrane, so there is no difference between FFPFF, ATN-FFPFF and the competitive inhibition group.

In the next experiment, we observed how DOX was internalized by cells at different incubation time. As shown in Fig. 6F and G, the amount of DOX entering the cells gradually increased in the first 4 hours. The superimposed yellow fluorescence presents much more brilliant in 4 h than that in 2 h. However at 8 h, the fluorescence intensity of DOX decreases, and the fluorescence of DOX and Lysotracker no longer overlaps, which is the same for both carriers. This indicates that after 8 hours of incubation, DOX is gradually metabolized by cells, and almost all DOX escapes from endosomes.

3.6 Antitumor *in vitro* with the drug-loaded polymers

In this study, we used the WST-1 kit and flow cytometry (FACS) to detect the proliferation inhibition and promotion of apoptosis in MDA-MB-231 cells, as shown in Fig. 7. The drug-loaded group was able to inhibit the proliferation of MDA-MB-231 cells, and free-DOX group had the best inhibitory effect with an inhibition rate of 49.34%. The inhibition rate of free-ATN + ATN-FFPFF-ATN-DOX was about 48.74%, while the rates of the FFPFF-DOX and ATN + ATN-FFPFF-ATN-DOX groups were 26.56% and 26.01%, respectively. Results of flow cytometry are shown in Fig. 8. Compared to the control group, the four

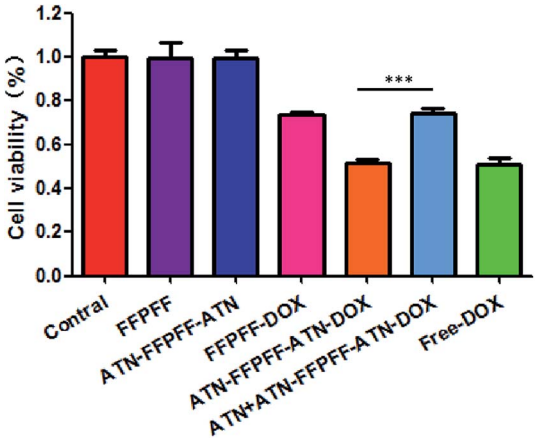

Fig. 7 WST-1 kit detected the proliferation inhibition at 24 h. The inhibition experiment was carried out by using free ATN-161 to pre-treated cells for 4 h before adding ATN-FFPFF-ATN-DOX. MDA-MB-231 cells incubates with formulations (DOX 20 μg mL^{-1}) in 4 h. Then replace with a new medium and continue culturing for 20 hours. Data are presented as the average ±SD ($n = 6$). *$p < 0.05$, **$p < 0.01$, ***$p < 0.001$.

experimental groups significantly promoted the apoptosis of MDA-MB-231 cells. Among them, ATN-FFPFF-ATN-DOX had the best effect of promoting tumor cell apoptosis, with a cell apoptosis rate of 26.31%, followed by the free-DOX group, in which the rate was 23.65%. The FFPFF-DOX group and the ATN + ATN-FFPFF-ATN-DOX groups exhibited values of 12.13 and 11.04%, respectively. ATN-FFPFF-ATN-DOX had the best effect of promoting tumor cell apoptosis, due to the gradually decomposing after drug delivery into cells. During this period, the effect of the drug was maximum; therefore, prolonging its action in tumor cells could has a better effect on inhibiting tumor cell proliferation and promoting apoptosis.

4. Conclusions

In this study, we designed and synthesized two pH-responsive drug carriers, FFPFF and ATN-FFPFF-ATN. ANT-161 peptide selectively increased the internalization of integrin $\alpha_5\beta_1$-positive cells. Moreover, at pH 5.5, the disintegration of the material was able to release a large amount of DOX. These specific selections for tumor cells increased their ability to kill tumor cells. In summary, ATN-FFPFF-ATN are potential carriers for targeted delivery of DOX to treat breast cancer.

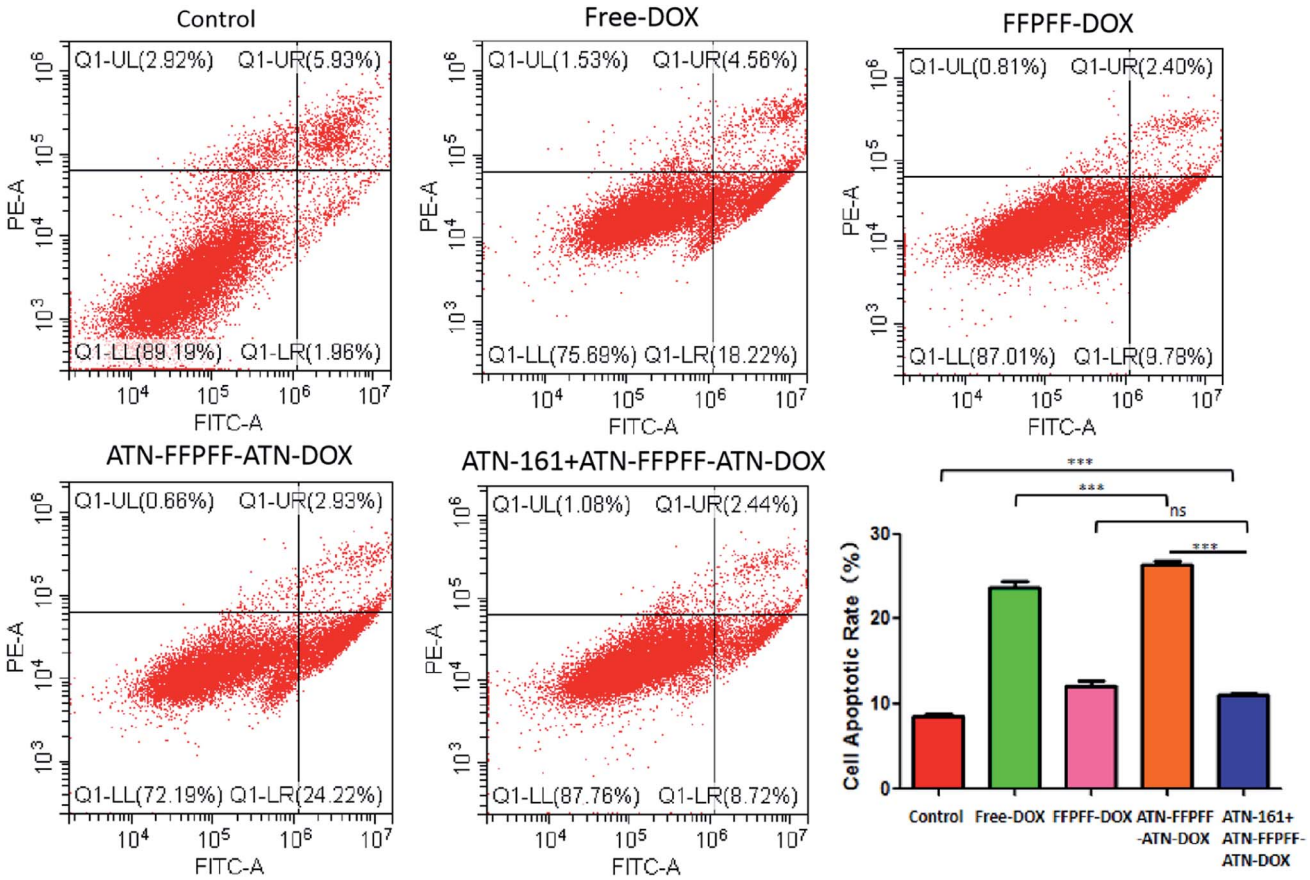

Fig. 8 Flow cytometry to detect the promotion of apoptosis of MDA-MB-231 cells. The inhibition experiment was carried out by using free ATN-161 pretreating cells for 4 h before adding FFPFF-DOX, ATN-FFPFF-ATN-DOX or free-DOX. MDA-MB-231 cells incubates with formulations (DOX 20 μg mL^{-1}) in 4 h. Then replace with a new medium and continue culturing for 20 hours. Data are presented as the average ±SD ($n = 3$). *$p < 0.05$, **$p < 0.01$, ***$p < 0.001$.

Conflicts of interest

There are no conflicts to declare.

Acknowledgements

This work was supported by the National Natural Science Foundation of China (no. 31401086), and the Science and Technology Development Program of Jilin Province, China (no. 20200404114YY).

References

1 R. L. Siegel, K. D. Miller and A. Jemal, Cancer statistics, *Ca-Cancer J. Clin.*, 2020, **70**(1), 7–30.

2 S. Niu, G. R. Williams, J. Wu, *et al.* A novel chitosan-based nanomedicine for multi-drug resistant breast cancer therapy, *Chem. Eng. J.*, 2019, **369**, 134–149.

3 D. Vyas, N. Lopez-Hisijos, S. Gandhi, M. El-Dakdouki, M. D. Basson, M. F. Walsh, X. Huang, A. K. Vyas and L. S. Chaturvedi, Doxorubicin-Hyaluronan Conjugated Super-Paramagnetic Iron Oxide Nanoparticles (DOX-HA-SPION) Enhanced Cytoplasmic Uptake of Doxorubicin and Modulated Apoptosis, IL-6 Release and NF-kappaB Activity in Human MDA-MB-231 Breast Cancer Cells, *J. Nanosci. Nanotechnol.*, 2015, **15**(9), 6413–6422.

4 S. Rai, R. Paliwal and S. P. Vyas, Doxorubicin encapsulated nanocarriers for targeted delivery to estrogen responsive breast cancer, *J. Biomed. Nanotechnol.*, 2011, **7**(1), 121–122.

5 Z. Y. Zhang, Y. D. Xu, Y. Y. Ma, L. L. Qiu, Y. Wang, J. L. Kong and H. M. Xiong, Biodegradable ZnO@polymer core-shell nanocarriers: pH-triggered release of doxorubicin in vitro, *Angew. Chem., Int. Ed.*, 2013, **52**(15), 4127–4131.

6 C. Nazli, G. S. Demirer, Y. Yar, H. Y. Acar and S. Kizilel, Targeted delivery of doxorubicin into tumor cells via MMP-sensitive PEG hydrogel-coated magnetic iron oxide nanoparticles (MIONPs), *Colloids Surf., B*, 2014, **122**, 674–683.

7 T. Wang, J. Hou, C. Su, L. Zhao and Y. Shi, Hyaluronic acid-coated chitosan nanoparticles induce ROS-mediated tumor cell apoptosis and enhance antitumor efficiency by targeted drug delivery via CD44, *J. Nanobiotechnol.*, 2017, **15**(1), 7.

8 E. Doolittle, P. M. Peiris, G. Doron, A. Goldberg, S. Tucci, S. Rao, S. Shah, M. Sylvestre, P. Govender, O. Turan, Z. Lee, W. P. Schiemann and E. Karathanasis, Spatiotemporal Targeting of a Dual-Ligand Nanoparticle to Cancer Metastasis, *ACS Nano*, 2015, **9**(8), 8012–8021.

9 A. N. Koo, H. J. Lee, S. E. Kim, J. H. Chang, C. Park, C. Kim, J. H. Park and S. C. Lee, Disulfide-cross-linked PEG-poly(amino acid)s copolymer micelles for glutathione-mediated intracellular drug delivery, *Chem. Commun.*, 2008, (48), 6570–6572.

10 M. Najafi, N. H. Goradel, B. Farhood, E. Salehi, S. Solhjoo, H. Toolee, E. Kharazinejad and K. Mortezaee, Tumor microenvironment: Interactions and therapy, *J. Cell. Physiol.*, 2019, **234**(5), 5700–5721.

11 F. Mpekris, C. Voutouri, P. Papageorgis, *et al.* Stress alleviation strategy in cancer treatment: Insights from a mathematical model, *Z. Angew. Math. Mech.*, 2018, **98**(12), 2295–2306.

12 T. G. Simonsen, K. V. Lund, T. Hompland, G. B. Kristensen and E. K. Rofstad, DCE-MRI-Derived Measures of Tumor Hypoxia and Interstitial Fluid Pressure Predict Outcomes in Cervical Carcinoma, *Int. J. Radiat. Oncol., Biol., Phys.*, 2018, **102**(4), 1193–1201.

13 D. Zhang, L. Li, X. Ji, *et al.* Intracellular GSH-responsive camptothecin delivery systems, *New J. Chem.*, 2019, **43**, 18673–18684.

14 Y. Bae, N. Nishiyama, S. Fukushima, H. Koyama, M. Yasuhiro and K. Kataoka, Preparation and biological characterization of polymeric micelle drug carriers with intracellular pH-triggered drug release property: tumor permeability, controlled subcellular drug distribution, and enhanced *in vivo* antitumor efficacy, *Bioconjugate Chem.*, 2005, **16**(1), 122–130.

15 Y. Hu, C. Yu, H. Zhang, J. Wang, G. Jiang and C. Kan, pH-Triggered Drug Release of Monodispersed P(St-co-DMAEMA) Nanoparticles: Effects of Swelling, Polymer Chain Flexibility and Drug-Polymer Interactions, *J. Nanosci. Nanotechnol.*, 2017, **17**(2), 900–907.

16 N. M. Matsumoto, G. W. Buchman, L. H. Rome and H. D. Maynard, Dual pH- and Temperature-Responsive Protein Nanoparticles, *Eur. Polym. J.*, 2015, **69**, 532–539.

17 G. Verma, N. G. Shetake, K. C. Barick, *et al.* Covalent immobilization of doxorubicin in glycine functionalized hydroxyapatite nanoparticles for pH-responsive release, *New J. Chem.*, 2018, 6283–6292.

18 L. Ding, Y. Jiang, J. Zhang, H. A. Klok and Z. Zhong, pH-Sensitive Coiled-Coil Peptide-Cross-Linked Hyaluronic Acid Nanogels: Synthesis and Targeted Intracellular Protein Delivery to CD44 Positive Cancer Cells, *Biomacromolecules*, 2018, **19**(2), 555–562.

19 M. Fu, C. Zhang, Y. Dai, X. Li, M. Pan, W. Huang, H. Qian and L. Ge, Injectable self-assembled peptide hydrogels for glucose-mediated insulin delivery, *Biomater. Sci.*, 2018, **6**(6), 1480–1491.

20 X. Xu, J. D. Flores and C. L. Mccormick, Reversible Imine Shell Cross-Linked Micelles from Aqueous RAFT-Synthesized Thermoresponsive Triblock Copolymers as Potential Nanocarriers for "pH-Triggered" Drug Release, *Macromolecules*, 2011, **44**(6), 1327–1334.

21 S. J. Lee, K. H. Min, H. J. Lee, A. N. Koo, H. P. Rim, B. J. Jeon, S. Y. Jeong, J. S. Heo and S. C. Lee, Ketal cross-linked poly(ethylene glycol)-poly(amino acid)s copolymer micelles for efficient intracellular delivery of doxorubicin, *Biomacromolecules*, 2011, **12**(4), 1224–1233.

22 N. Liu, J. Han, X. Zhang, Y. Yang, Y. Liu, Y. Wang and G. Wu, pH-responsive zwitterionic polypeptide as a platform for anti-tumor drug delivery, *Colloids Surf., B*, 2016, **145**, 401–409.

23 N. Gao, L. Shaoyu and G. Chunmei, Injectable shell-crosslinked F127 micelle/hydrogel composites with pH and

redox sensitivity for combined release of anticancer drugs, *Chem. Eng. J.*, 2016, **287**, 20–29.

24 J. Yang, Y. Huang, C. Gao, M. Liu and X. Zhang, Fabrication and evaluation of the novel reduction-sensitive starch nanoparticles for controlled drug release, *Colloids Surf., B*, 2014, **115**, 368–376.

25 J. Yang, C. Gao, S. Lü, X. Zhang, C. Yu and M. Liu, Physicochemical characterization of amphiphilic nanoparticles based on the novel starch-deoxycholic acid conjugates and self-aggregates, *Carbohydr. Polym.*, 2014, **102**, 838–845.

26 Y. Jinlong, G. Chunmei, L. Shaoyu, *et al.* Novel self-assembled amphiphilic mPEGylated starch-deoxycholic acid polymeric micelles with pH-response for anticancer drug delivery, *RSC Adv.*, 2014, 55139–55149.

27 C. Wu, J. Yang, X. Xu, *et al.* Redox-responsive core-cross-linked mPEGylated starch micelles as nanocarriers for intracellular anticancer drug release, *Eur. Polym. J.*, 2016, **83**, 230–243.

28 B. A. Cisterna, N. Kamaly, W. I. Choi, A. Tavakkoli, O. C. Farokhzad and C. Vilos, Targeted nanoparticles for colorectal cancer, *Nanomedicine*, 2016, **11**(18), 2443–2456.

29 M. Reches and E. Gazit, Casting metal nanowires within discrete self-assembled peptide nanotubes, *Science*, 2003, **300**(5619), 625–627.

30 X. Yan, Q. He, K. Wang, L. Duan, Y. Cui and J. Li, Transition of cationic dipeptide nanotubes into vesicles and oligonucleotide delivery, *Angew. Chem., Int. Ed.*, 2007, **46**(14), 2431–2434.

31 S. Guan, X. Yu, J. Li, *et al.* Delivery of Survivin siRNA Using Cationic Diphenylalanine Vesicles, *Chem. Res. Chin. Univ.*, 2019, **35**(2), 434–439.

32 W. Han, Y. Yuan, H. Li, Z. Fu, M. Wang, S. Guan and L. Wang, Design and anti-tumor activity of self-loaded nanocarriers of siRNA, *Colloids Surf., B*, 2019, **183**, 110385.

33 O. Stoeltzing, W. Liu, N. Reinmuth, F. Fan, G. C. Parry, A. A. Parikh, M. F. McCarty, C. D. Bucana, A. P. Mazar and L. M. Ellis, Inhibition of integrin alpha5beta1 function with a small peptide (ATN-161) plus continuous 5-FU infusion reduces colorectal liver metastases and improves survival in mice, *Int. J. Cancer*, 2003, **104**(4), 496–503.

34 W. Dai, T. Yang, X. Wang, J. Wang, X. Zhang and Q. Zhang, PHSCNK-Modified and doxorubicin-loaded liposomes as a dual targeting system to integrin-overexpressing tumor neovasculature and tumor cells, *J. Drug Targeting*, 2010, **18**(4), 254–263.

35 N. Zhang, Y. Xia, Y. Zou, W. Yang, J. Zhang, Z. Zhong and F. Meng, ATN-161 Peptide Functionalized Reversibly Cross-Linked Polymersomes Mediate Targeted Doxorubicin Delivery into Melanoma-Bearing C57BL/6 Mice, *Mol. Pharm.*, 2017, **14**(8), 2538–2547.

36 T. F. Yang, C. N. Chen, M. C. Chen, C. H. Lai, H. F. Liang and H. W. Sung, Shell-crosslinked Pluronic L121 micelles as a drug delivery vehicle, *Biomaterials*, 2007, **28**(4), 725–734.

37 D. Zukancic, E. J. A. Suys, E. H. Pilkington, A. Algarni, H. Al-Wassiti and N. P. Truong, The Importance of Poly(ethylene glycol) and Lipid Structure in Targeted Gene Delivery to Lymph Nodes by Lipid Nanoparticles, *Pharmaceutics*, 2020, **12**(11), 1068.

38 H. Saito, A. S. Hoffman and H. I. Ogawa, Delivery of Doxorubicin from Biodegradable PEG Hydrogels Having Schiff Base Linkages, *J. Bioact. Compat. Polym.*, 2007, **22**(6), 589–601.

39 Z. Gong, X. Liu, J. Wu, X. Li, Z. Tang, Y. Deng, X. Sun, K. Chen, Z. Gao and J. Bai, pH-triggered morphological change in a self-assembling amphiphilic peptide used as an antitumor drug carrier, *Nanotechnology*, 2020, **31**(16), 165601.

40 M. N. Vu, H. G. Kelly, A. K. Wheatley, S. Peng, E. H. Pilkington, N. A. Veldhuis, T. P. Davis, S. J. Kent and N. P. Truong, Cellular Interactions of Liposomes and PISA Nanoparticles during Human Blood Flow in a Microvascular Network, *Small*, 2020, **16**(33), e2002861, DOI: 10.1002/smll.202002861Epub 2020 Jun 25. PMID: 32583981; PMCID: PMC7361276.